Limnol. Oceanogr., 45(7), 2000, 1621–1638

Seasonal evolution of the basin-scale internal wave field in a large stratified lake

Jason P. Antenucci,[1] *Jörg Imberger, and Angelo Saggio*
Department of Environmental Engineering, Centre for Water Research, University of Western Australia, Nedlands, 6907 Australia

Abstract

The response of the water column to varying conditions of stratification and wind forcing was investigated in Lake Kinneret (Israel) using data collected from thermistor chains and acoustic Doppler current profilers during 1997 and 1998. The strong daily sea breeze was found to generate a vertical mode 1 internal Kelvin wave and basin-scale internal Poincaré waves of vertical modes 1, 2, and 3. The Kelvin wave, the dominant component of the internal wave field, was responsible for alongshore velocities in the nearshore regions. In the upwind nearshore regions, velocities were dominated by the forced response to the wind and were cross-shore in nature. In the lake interior, the Kelvin wave effect on the horizontal velocity field was minor compared to the higher vertical mode Poincaré waves. The Kelvin wave is shown to exist in resonant and nonforced states with the wind, whereas the vertical mode 1 Poincaré wave energy remained relatively constant, despite large variability in the forcing conditions. The energy in the higher mode Poincaré waves varied greatly, both on daily and seasonal timescales. The results demonstrate that the wind energy forces multiple basin-scale internal wave modes and that prior motion in the water column must be considered when determining the subsequent internal wave response in periodically forced systems.

Lake Kinneret (Israel) has long been an important regional resource, providing a substantial supply of drinking water as well as supporting a commercial fishery. The monomictic lake is forced daily during the summer by a powerful sea breeze, with stratification and wind patterns showing little variation from year to year. These factors, along with a favorable bathymetric pattern, combine to make Lake Kinneret an ideal place for the field investigation of large-scale internal waves and related phenomena such as the benthic boundary layer, horizontal transport, and vertical mixing processes. In addition to providing substantial insight into the local processes—and hence, influencing local management—study of the lake also provides fundamental knowledge of the dynamics of enclosed basins on a geophysical scale.

During summer, the internal Rossby radius in Lake Kinneret is typically one-half the basin width; hence, large-scale motion in the lake will be affected by the earth's rotation, and basin-scale internal waves may be of topographic Rossby, Kelvin, or Poincaré form. Topographic Rossby waves are sub–inertial frequency oscillations that exist only in rotating fluids with variable bathymetry (Mysak et al. 1985; Stocker and Hutter 1987), and these waves result from changes in depth affecting the relative vorticity of fluid elements. In the absence of vertical boundaries, wavelike solutions to the linear inviscid equations of motion for a flat-bottomed region of homogeneous fluid with a constant rate of rotation are known as plane progressive Poincaré waves (Gill 1982). The structure of these waves is similar to that of nonrotating waves, with the addition of elliptical particle orbits in the horizontal plane that rotate clockwise in the Northern Hemisphere. The introduction of a single vertical boundary requires the interaction of an incident Poincaré wave with its perfect reflection in order to satisfy the boundary condition of no normal motion at the boundary (LeBlond and Mysak 1978). The second possible solution to the linear equations is a Kelvin wave, which results from an exponential offshore decay of pressure being balanced by the Coriolis force. The decay scale of the wave is the Rossby radius c/f (i.e., the phase speed divided by the inertial frequency). The wave propagates along the coastline, with the shore to the right in the Northern Hemisphere and zero normal velocity throughout the domain (Gill 1982). The Kelvin wave solution is readily satisfied with the addition of a second parallel vertical boundary, forming a channel of arbitrary width as a result of the zero normal velocity. For the reflected Poincaré solution to satisfy the boundary conditions imposed by a channel, the cross-channel wave number of the Poincaré wave must be limited to the set $n\pi/L$, where n is an integer representing the horizontal mode and L is the width of the channel. The resultant wave is known as a progressive Poincaré wave (Gill 1982). Standing Poincaré wave solutions can be constructed with the addition of two identical progressive Poincaré waves propagating in opposite directions (Mortimer 1974). Such standing waves have a cellular structure, with the cell dimension being one horizontal mode in both horizontal directions. Velocities within the cell are maximal at the cell center and zero at the cell boundary, with velocities in neighboring cells that are oppositely directed.

Internal wave activity was first recorded in Lake Kinneret by Serruya (1975), who related the magnitude of the metalimnetic displacement to the magnitude of the wind. Isotherm displacements on opposite sides of the lake were out of phase, with a nodal point in the center of the lake. Dominant

[1] Corresponding author (antenucc@cwr.uwa.edu.au).

Acknowledgments

The first author was the recipient of an Australian postgraduate award and an F. S. Shaw Memorial postgraduate scholarship. The fieldwork was supported by the Centre for Environmental Fluid Dynamics and the Yigal Allon Kinneret Limnological Laboratory (KLL). The assistance of James Easton and Miki Shlichter from KLL is gratefully acknowledged. The authors thank Ben Hodges and Greg Ivey for comments on an earlier version of this manuscript. This paper represents Centre for Water Research reference ED 1262-JA.

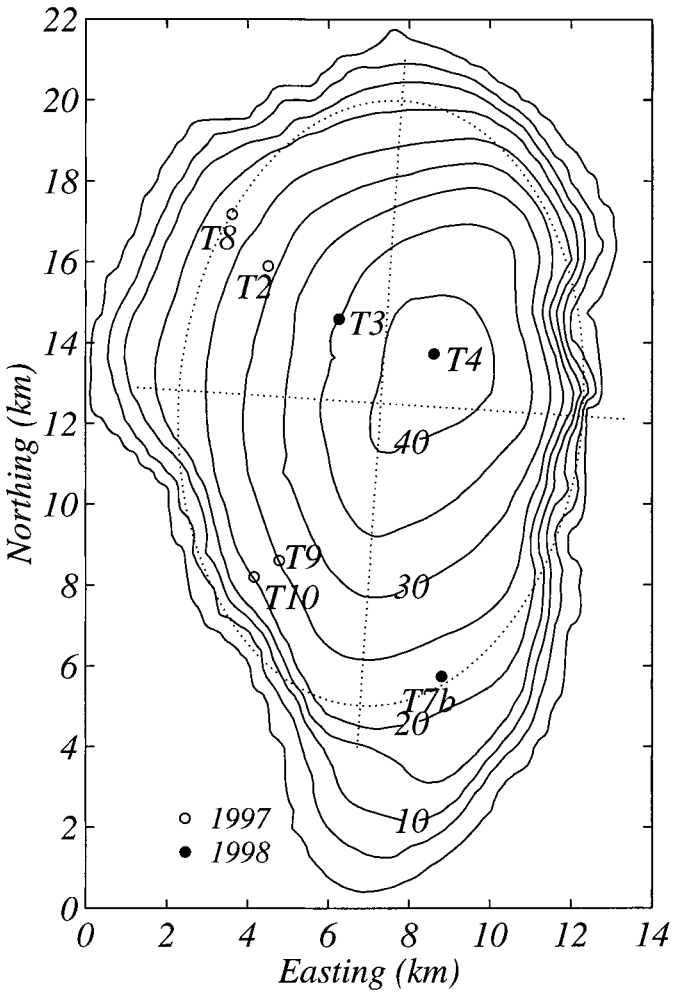

Fig. 1. Lake Kinneret bathymetry with location of relevant sampling stations during the 1997 and 1998 experiments. ADCPs were deployed at Sta. T3, T8, and T10. Thermistor chains were deployed at all stations except T8 and T10. Sta. T2, T3, and T4 are aligned along the primary wind axis. An ellipse of aspect ratio of 2 to 3 (10,000 m : 15,000 m) is superimposed for use in the discussion. The origin of the map grid is situated at 35.51°N, 32.70°E.

frequencies at 24 and 12 h were observed, with the 24-h wave (1) found to propagate anticlockwise and (2) attributed to the daily wind forcing. The 12-h wave was attributed to ''a natural free period of oscillation, probably of the third (horizontal) mode.'' The 24-h oscillation was identified by Ou and Bennett (1979) to be a vertical mode 1 internal Kelvin wave, with the 12-h component of the signal identified as a vertical mode 1, horizontal mode 1 internal seiche (i.e., nonrotating). Investigations by Ostrovsky et al. (1996) indicated the presence of both a vertical mode 1 and a mode 2 component of the basin-scale seiche.

The strong daily sea breeze that acts over Lake Kinneret is a seasonal phenomenon (Neumann and Stanhill 1978), so substantial seasonal differences in the internal wave field are expected as changing stratification affects the partitioning of energy among vertical modes (Stevens and Lawrence 1997). Given the role of the internal wave field in distributing energy and momentum (Saggio and Imberger 1998), on mixing at the boundaries (Ivey and Nokes 1989; Michallet and Ivey 1999), and in generation of the benthic boundary layer (Lemckert and Imberger 1998), the investigation of the seasonal behavior of internal waves in Lake Kinneret becomes important, as these variables determine the physical regime under which the biogeochemical system must operate (Nishri et al. 2000).

Table 1. Details of deployments in 1997 and 1998 experiments (TC = thermistor chain).

Sta.	Instrument	Year	Period	Sampling interval	Depth range
T2	TC	1997	Jun 14–Jul 01	10 s	Full
T3	TC	1998	Jun 27–Jul 10	10 s	Full
T3	TC	1998	Jul 11–Aug 06	30 s	Full
T3	TC	1998	Sep 08–Oct 14	30 s	Full
T3	ADCP	1998	Jul 05–Jul 13	15 min	8–22 m
T4	TC	1998	Jun 27–Jul 10	10 s	Full
T7b	TC	1998	Jun 27–Jul 10	120 s	Full
T8	ADCP	1997	Jun 17–Jun 26	60 min	9–16 m
T9	TC	1997	Jun 13–Jul 01	120 s	Full
T10	ADCP	1997	Jun 27–Jul 01	60 min	11–18 m

The focus of the present study is to identify and characterize the basin-scale internal wave field using data from experiments carried out in June 1997 and July–October 1998. An analytical solution to the basin-scale internal wave response is derived and is shown to closely approximate the measured response. Seasonal evolution of the amplitude and phase of these waves is then discussed using a simple resonance model and data from the 1998 experiment.

Methods

The site for the field investigation was Lake Kinneret, Israel (Fig. 1). The lake is approximately 22 by 15 km, is oriented in a north–south direction, and has a maximum depth of 42 m and a surface area of 167 km^2. During the months of April to October, a daily westerly sea breeze commences soon after midday, and this breeze lasts for 5–8 h and reaches speeds of 15 m s^{-1} at 10 m above the water surface. The onset of the wind is sudden, with the wind speed increasing from 1 or 2 m s^{-1} to 10 m s^{-1} in less than 10 min. The water column remains stratified from late February through late December. Inflows and outflows during the stratified seasons were negligible during the study period, and the density variation due to salinity was minor.

Those details of the field deployments that are relevant to this study are presented in Table 1. Temperature data were collected with arrays of 20 thermistors (to an accuracy of 0.01°C) during both experiments. Spacing of the thermistors was 1 m in the metalimnion, with greater intervals in the hypolimnion and epilimnion. Velocity data were collected with orthogonal pairs of 1.25-MHz coherent acoustic Doppler current profilers (ADCP) (Bugnon and Whitehouse 1991), with a spatial resolution of 150 mm and velocity resolutions of 1 cm s^{-1} (1997) and 0.25 cm s^{-1} (1998). Sta. T3 (1998) was fitted with a wind anemometer and direction sensor (ca. 1.5 m above the surface of the water) that sampled

at the same frequency as the thermistors. Subsequent analysis of the wind data focuses on 10-min averages, with wind data corrected to 10-m elevation (Amorocho and DeVries 1980).

The standard method of investigating the frequency content of an internal wave field involves spectral analysis of isotherm or isopycnal displacements (*see* Phillips [1977], Garrett and Munk [1979], and Lemmin [1987]). Although it is clear that this technique is successful in identifying dominant frequencies, it is difficult to make a connection between the isotherm displacement and the energy contained in the internal wave field. Moum et al. (1992) calculated potential energy as $N^2\langle\zeta^2\rangle$, where ζ is the root mean square (r.m.s.) displacement of an isotherm; however, one must make a subjective selection of a representative isotherm. Further, spectral techniques do not yield phase details, and so time frequency information is lost, and thus it is not possible to distinguish wave groups from a spectrum of waves.

For these reasons, the internal wave field was analyzed using both power spectra and wavelet transforms of the integrated potential energy time series, where the integrated potential energy was calculated as

$$PE(t) = \int_{Z_0}^{H} \rho(z, t) g z \, dz. \tag{1}$$

This gave a much clearer picture of the frequency content of the internal wave field and also of the relative distribution of potential energy among frequencies. Using such a measure to determine characteristics of the internal wave field removed the uncertainty of choosing a representative isotherm on a seasonal timescale.

The integrated potential energy signal magnifies the vertical mode 1 components of the signal relative to higher vertical modes. Vertical mode 1 motion involves lifting the whole water column up and down, whereas higher vertical modes involve lifting only part of the water column while the other part of the column is depressed. The result is that a vertical mode 1 wave will show a greater contribution to the integrated potential energy than will a higher vertical mode wave of the same frequency and amplitude. This can be shown by estimating the density perturbation due to a long linear internal wave of amplitude A_m, angular frequency ω_m, phase ϕ_m, and vertical velocity eigenfunction w_m, as follows:

$$\rho'_m(z, t) = \frac{\rho_0 N^2(z)}{g} \frac{A_m w_m(z)}{\omega_m} \sin(\omega_m t + \phi_m), \tag{2}$$

where the vertical velocity eigenfunctions are determined through solution of the long linear internal wave problem in a rotating system (LeBlond and Mysak 1978),

$$\frac{d^2 w_m(z)}{dz^2} + \frac{N^2(z)}{c_m^2} w_m(z) = 0. \tag{3}$$

This applies for both Kelvin and Poincaré solutions, with $c^2 = g'h$ for Kelvin wave solutions and $c^2 = (\omega^2 - f^2)/(k^2 + l^2)$ for Poincaré waves (Gill 1982).

For a linearly stratified case, the integrated potential energy ratio between waves i and j of the same frequency and amplitude is n_j/n_i, where n is the vertical mode of the wave. To demonstrate the effect for a more representative stratification, vertical velocity eigenfunctions were found by solving Eq. 3 for the stratification in Lake Kinneret during early July 1998. Waves of 24-h period of the same amplitude but different vertical mode were then generated separately using Eq. 2, and the time series of integrated potential energy was calculated. The vertical mode 1 wave was found to have more than one order of magnitude greater power than any other vertical mode at the frequency of interest.

The integrated potential energy time series calculated using Eq. 1 were first analyzed using standard Fourier power spectral methods, with estimates averaged in the frequency domain to improve confidence. A time-frequency analysis was then carried out using wavelet transforms. The mother wavelet used was of the Morlet form,

$$\psi(t) = \exp\left(-\frac{t^2}{2}\right)\cos 5t. \tag{4}$$

The continuous wavelet transform of a signal $f(t)$ is defined by Kaiser (1994) as

$$c(s, t) = \int_{-\infty}^{\infty} f(u)\psi_{s,t}(u) \, du, \tag{5}$$

where

$$\psi_{s,t}(u) = \frac{1}{\sqrt{s}}\psi\left(\frac{u - t}{s}\right). \tag{6}$$

The coefficient c represents the characteristics of the signal at scale s. The mother wavelet chosen has a well-defined frequency, and so a transformation between scales and frequency can be made as follows

$$f = \frac{5}{2\pi s h}, \tag{7}$$

where h is the sampling interval of the time series, and s the scale of the mother wavelet.

Although the integrated potential energy signal provides information on wave power, it is not suitable for the determination of the vertical modal structure. Previous work has identified higher vertical mode oscillations through the use of cross-correlation techniques between time series of isotherm displacements (Wiegand and Chamberlain 1987; Roget et al. 1993). This approach assumes that the energy at a particular frequency is attributable to a single wave; unfortunately, this is not the case in Lake Kinneret, where basin-scale baroclinic responses of differing vertical modes at similar frequencies occur (*see following section*). In order to determine the partitioning of energy among the vertical modes, we fitted vertical eigenfunctions to perturbations in the density field in a manner similar to that used by Webb and Pond (1986) and Thorpe and Jiang (1998). The density field in the lake was estimated as

$$\tilde{\rho}(z, t) = \bar{\rho}(z) + \sum_{m=1}^{M} \rho'_m(z, t). \tag{8}$$

The prime refers to the fluctuating component of the density

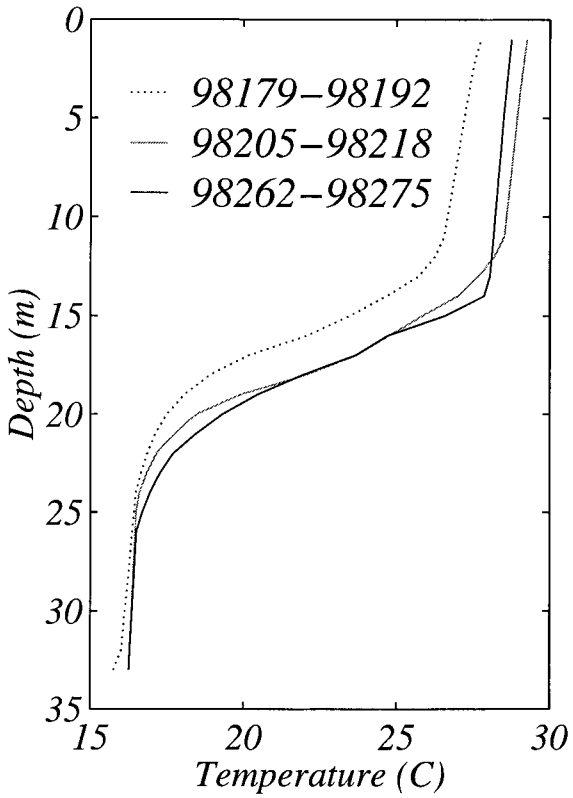

Fig. 2. Background stratification, calculated as the average depth of the isotherms during the period (Thorpe et al. 1996) for the three analysis periods in 1998.

field defined in Eq. 2, whereas the overbar represents the background density profile. A set of M linear waves, each with vertical eigenfunction $w_m(z)$ and frequency ω_m, was selected. By fitting the above equation to the measured density field, it was possible to determine the amplitudes and phases (A_m, ϕ_m) of the selected waves.

Equation 8 was fitted to the field data on a daily basis, beginning at midday and continuing through to the following midday. The background stratification was determined for each daily window by finding the average depth of isotherms during the given period (Thorpe et al. 1996), from which the buoyancy frequency profile $N^2(z)$ was calculated. Based on the frequency analysis, a set of waves ($w_m(z)$, ω_m) was chosen, and the eigenvalue problem in Eq. 3 was solved to determine the form of the vertical eigenfunctions. Amplitudes and phases (A_m, ϕ_m) were then determined using a least-squares fitting method.

Table 3. Three-homogeneous layer approximation to the stratification in Fig. 2, with layer boundaries defined as the depth at which the temperature gradient fell below -0.5°C m^{-1} for the surface layer or rose above -0.5°C m^{-1} for the middle layer (z defined positive down). The thickness of the bottom layer was calculated as the difference in height between the base of the middle layer and the average depth of the basin below the base of the middle layer. The temperature of each layer was calculated as the volume average over the layer thickness.

Period	h_1 (m)	h_2 (m)	h_3 (m)	θ_1 (°C)	θ_2 (°C)	θ_3 (°C)
98179-192	12.5	8	6	27.0	21.1	16.6
98205-218	12.5	10	5.5	28.8	22.4	16.6
98262-275	14.5	8.5	5.5	28.3	21.3	16.7

General features of the wind forcing and water column response

Three periods were investigated during the 1998 experiment; the selected periods covered the gradual heating and cooling of the lake. The first period extended from 28 Jun to 11 Jul (98179-98192), the second from 24 Jul to 6 Aug (98205-98218), and the third period from 19 Sep to 2 Oct (98262-98275). The two deployment periods were from days 98178 to 98218 and from days 98251 to 98287. The temperature structure during the three analysis periods is shown in Fig. 2.

The bulk characteristics of the water column during the three periods are summarized in Tables 2 and 3. The first period was characterized by high wind stress, with the weakest stratification relative to the other two periods, as indicated by the vertical mode 1 phase speed. The largest isotherm displacements were observed during this time. The second period saw a negligible change in the applied wind stress and a significant increase in stratification. Wave amplitudes were typically lower during the second than during

Table 2. Bulk water column physical characteristics during the three periods showing η, the standard deviation of the displacement of the 23°C isotherm; the r.m.s. value of the wind speed at 10 m; u^*, the mean of the wind-induced shear velocity averaged over all daily wind events, where a daily wind event was defined as the time between the wind speed rising above the r.m.s. wind speed until the wind speed first dropped below the r.m.s. value; c_1, the long-wave linear phase speed based on a three-layer stratification (Table 3) for the first two vertical internal modes (Csanady 1982); W, the Wedderburn number, with the length scale taken as 11,000 m; L_N, the lake number; R, the Rossby radius of deformation for the first internal mode c_1/f, where the inertial frequency is 7.81×10^{-5} rad s^{-1} (T_i = 22.3 h).

Period	η (m)	r.m.s. u_{10} (m s^{-1})	u^* (m s^{-1})	c_1 (m s^{-1})	c_2 (m s^{-1})	W	L_N	R_1 (m)
98179-192	1.6	6.0	0.0120	0.33	0.16	1.3	0.4	4200
98205-218	0.57	5.7	0.0124	0.36	0.19	1.4	0.5	4600
98262-275	0.32	1.5	0.0028	0.37	0.16	39	14	4700

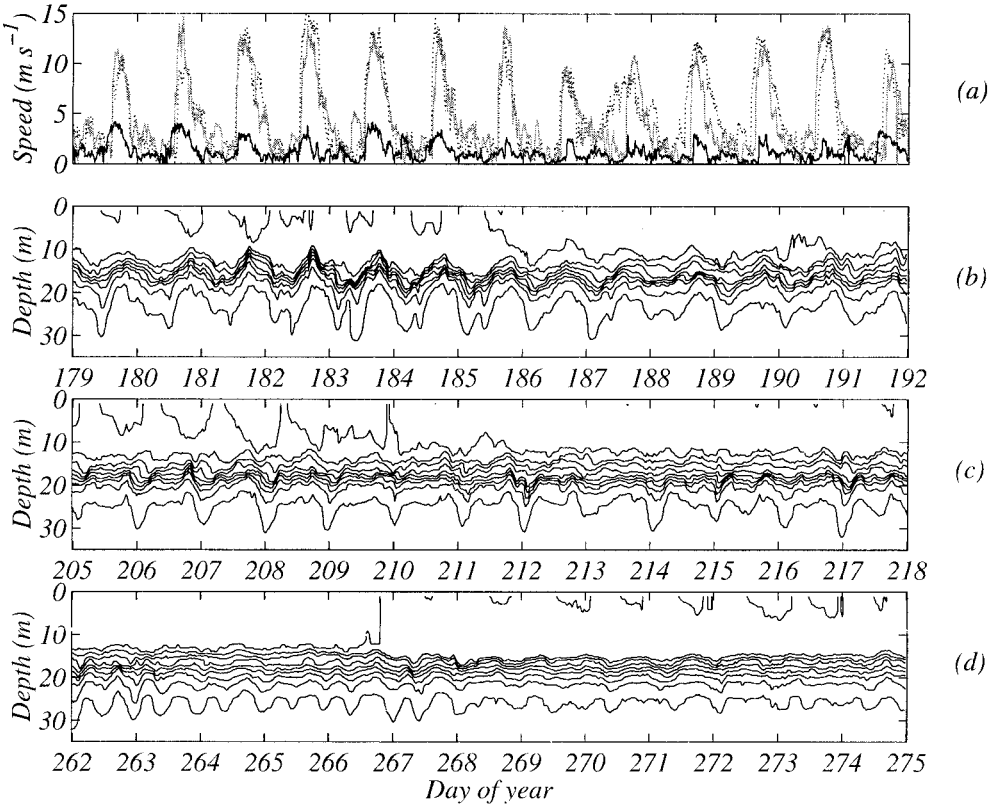

Fig. 3. Record of wind and isotherm displacement during the 1998 experiment for the three analysis periods measured at Sta. T3: (a) the 10-min average of wind corrected to 10 m above the water surface, for analysis periods 1–3 (light to dark shading); (b–d) isotherm response for periods 1–3. The bottom isotherm is 16.5°C, with a 1.5°C contour interval. Isotherms were calculated through linear interpolation and have been low–pass filtered at 1 h.

the first period. The third period was characterized by substantially lower wind stress and a slight increase in stratification. The change in the typical wave amplitudes was less pronounced.

The data from the Sta. T3 thermistor chain are presented in Fig. 3 along with the wind record for the three analysis periods. For the first period, the lake response was characterized by very large-amplitude vertical mode 1 waves of 24-h period and a vertical mode 1 12-h component, which occurred daily around 0800 h and which was visible in the troughs of the 24-h wave. The second period was characterized by smaller wave amplitudes, broader crests, and narrower troughs. The third period showed a definite 12-h oscillation up until day 268, after which time a weak 24-h vertical mode 1 oscillation again became apparent. Based on the isotherm response, it is clear that the decay timescale of the internal wave field was greater than 1 d.

The response of the water column during the three analysis periods may be parameterized on the basis of the values of the Wedderburn and Lake numbers (Stevens and Imberger 1996). The Wedderburn number is defined as

$$W = \frac{h_1}{L} Ri, \tag{9}$$

where h_1 is the surface layer depth, L the basin length, and Ri the bulk Richardson number c^2/u_*^2. The Lake number is defined as

$$L_N = \frac{M_{bc}}{\tau A z_v}, \tag{10}$$

where M_{bc} is the baroclinic moment about the center of volume, τ the surface stress, A the surface area, and z_v the depth to the center of volume. Low Lake numbers ($L_N < 1$) are associated with vertical mode 1 tilting of the metalimnion, whereas low Wedderburn numbers [$W < 1$, or O(1) if stratification is continuous—*see* Monismith 1986] are associated with upwind opening and downwind closing of the metalimnion, a vertical mode 2 response. High values of both numbers indicate calm conditions. During the first two periods, large vertical mode 1 excursions of the metalimnion are expected because of similar low values of L_N, whereas the third period should be characterized by small isotherm displacements predicted by a large L_N. Large vertical mode 2 motion in the metalimnion is also to be expected during the first two periods as a result of similar low values of W, whereas the vertical mode 2 response during the third period should be negligible because of the high value for W. The substantial decrease in the displacement of the 23°C isotherm between the first two periods (Table 2) remains unexplained by this parameterization. It will be shown later that rotational

effects, with the internal Rossby radius of deformation being smaller than the basin dimensions for all periods, and the periodic nature of the wind forcing were important in determining the isotherm response, requiring a modification of the simple steady-state L_N and W parameterizations.

The basin-scale internal wave field

Theoretical response—The natural frequencies of Lake Kinneret were estimated by approximating the lake as a circular basin of radius $r = 6$ km and uniform depth, with a stratification of three homogeneous layers (Table 3). The basin was rotated about its center at $0.5f$, where f was the inertial frequency at the latitude of Lake Kinneret (32.5°N). The linear solutions for a circular basin of uniform depth are given in Thomson (1879) and Lamb (1932), and the two-layer case is given in Csanady (1967). Extension of the problem to three layers was made by the method of normal modes (Csanady 1982; Monismith 1985) and is analogous to the two-layer problem. The method of normal modes is used to determine the nonrotating phase speed c for particular modes, which are then substituted into the generic single-layer problem.

Two classes of solution are possible: for superinertial frequencies, the solutions are Poincaré waves, and for subinertial frequencies, the solutions are Kelvin waves. Poincaré wave solutions can be found for all f, r, c, and n (horizontal mode), whereas Kelvin wave solutions are available for only a limited subset of n. Lamb (1932) showed that for a Kelvin wave solution of horizontal mode n to exist,

$$\beta > n(n + 1), \tag{11}$$

where

$$\beta = f^2 r^2 / c^2. \tag{12}$$

The parameter β represents the ratio of the period of travel of a long wave along a channel of length $2\pi r$ to the period of rotation of the water mass $2\pi/f$. For a long-wave nonrotating phase speed of 0.33 m s^{-1} (Table 2), $\beta = 2.0$ for our circular basin approximation to Lake Kinneret, and so only one vertical mode 1 internal Kelvin wave can be supported of the gravest horizontal mode.

Solutions are presented to the above problem for three waves: a vertical mode 1, horizontal mode 1 Kelvin wave; a vertical mode 1, horizontal mode 1 Poincaré wave; and a vertical mode 2, horizontal mode 1 Poincaré wave. The presence of these waves is identified in the field data (*see next section*), and so an understanding of their structure is useful. Using phase speeds during the first analysis period (Table 2) yields periods of 22.5, 12.2, and 17.5 h, respectively, for the three waves. The dynamical fields of these solutions—determined by substituting the modal pressure solution into the normal mode equations to determine modal velocities and then by transforming the modal fields into the layer fields, as in Csanady (1982)—are presented in Fig. 4. The Kelvin wave solution propagates anticlockwise, and the exponential decay usually associated with Kelvin waves (Gill 1982) is not apparent because the decay scale R_1 (Table 2) is approximately equal to the basin radius. The velocity fields for Kelvin waves show maxima at the boundaries (where the motion is rectilinear), with current vectors in the lake interior rotating anticlockwise. Poincaré solutions propagate clockwise, with interface displacements in phase for the vertical mode 1 motion and out of phase for the vertical mode 2 motion. Velocity vectors for the Poincaré solutions rotate clockwise, with maxima at the basin center. The velocity field due to the vertical mode 1 Kelvin and Poincaré waves is greatest in the upper and lower layers, whereas the velocity field due to the vertical mode 2 Poincaré wave is greatest in the middle and lower layers. All solutions are progressive but show a standing structure if measured only in cross section.

The circular basin solution raises the question of whether there is a critical condition at the inertial frequency for the basin-scale Kelvin waves. As β decreases because the heating of the lake increases the phase speed c, we could conceivably have a case in which the Kelvin wave is no longer supported (i.e., $\beta < 2$). This critical condition is simply a function of the circular basin solution. Goldstein (1929) showed that for an elliptic basin of uniform depth, a ''positive'' wave (one that propagates in the same sense as the rotation) can be both sub- and superinertial. The positive wave has a similar structure to that of the Kelvin wave shown in Fig. 4a,b, one that does not change as the frequency passes through the inertial frequency. Solving Goldstein's problem, assuming an aspect ratio of 2 : 3 in Lake Kinneret (Fig. 1), at the start of the stratification season, when $c = 0.33$ m s^{-1} (Table 2) and $\beta = 3.15$ (where a, one-half the major axis length, replaces r in Eq. 12, with $a = 7{,}500$ m), we find the ratio $\omega : f = 0.93$; thus, the Kelvin wave solution is subinertial. At the time of maximum stratification $c = 0.37$ m s^{-1} (Table 2) and $\beta = 2.5$, resulting in $\omega : f = 1.06$, a superinertial Kelvin wave. The Kelvin wave solution will return to a subinertial frequency as the epilimnion deepens and cools and as the phase speed c decreases below approximately 0.35 m s^{-1}.

Measured response—Power spectra of the integrated potential energy at Sta. T3 for all three analysis periods during 1998 showed significant peaks at 24, 12, and 6 h (Fig. 5). The energy peak at 6 h was not detected at Sta. T4 or T7b and so was not a coherent basin-scale motion.

Vertical mode 1 Kelvin wave: The energy at 24 h has been previously identified as a vertical mode 1 Kelvin wave by Ou and Bennett (1979). The velocity field associated with the Kelvin wave in the nearshore regions was available from ADCPs deployed during the 1997 experiment at Sta. T8 (Fig. 6) and T10 (Fig. 7). Kelvin waves are associated with velocities parallel to the boundary (Fig. 4a,b); however, velocities at Sta. T8 showed a strong cross-shore component of 24-h period. The onset of the wind was accompanied by the onset of water moving onshore at Sta. T8, and with the cessation of the wind, the water began to immediately move offshore. Velocities at this station showed a strong forced response to the wind, and so the velocity field associated with a freely propagating Kelvin wave (i.e., parallel to the boundary) was not observed. Once the forcing was released, the waves initialized by the forcing propagated freely, with the Kelvin wave progressing around the basin in an anti-

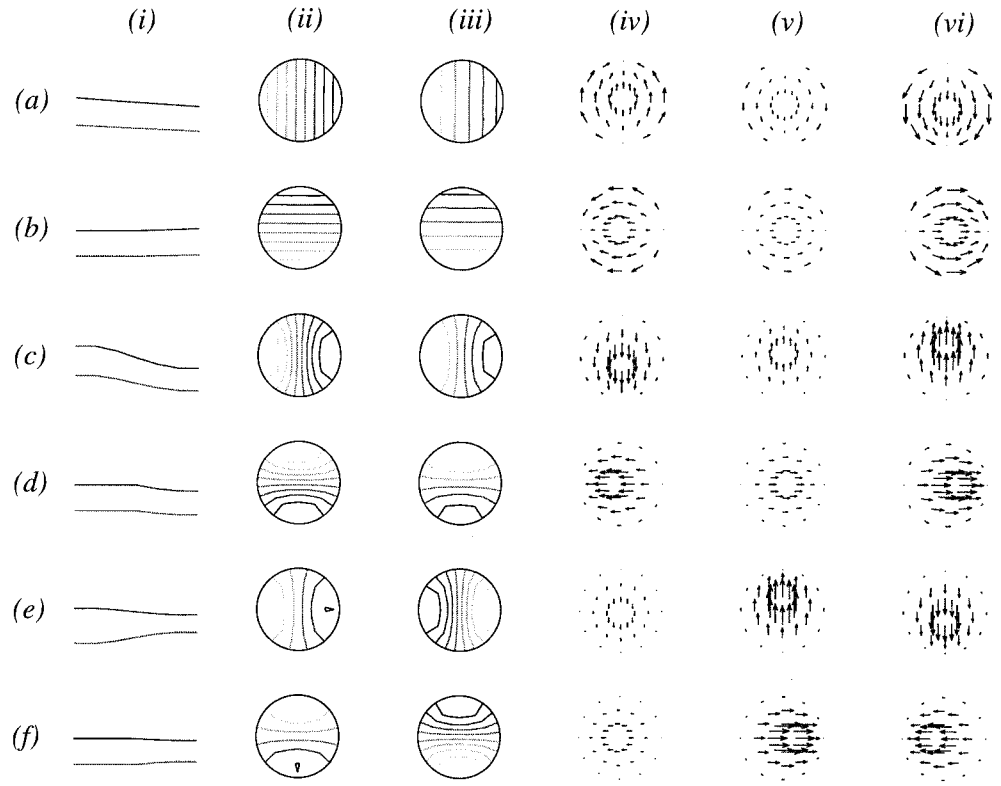

Fig. 4. Dynamical fields for a uniform-depth circular basin of 6-km radius situated at 32.5°N for the three-layer approximation in Table 3 during the first analysis period. The vertical mode 1, horizontal mode 1 Kelvin wave solution is shown in (a) and (b), for two times separated by $T/4$; the vertical mode 1, horizontal mode 1 Poincaré wave solution is shown in (c) and (d); and the vertical mode 2, horizontal mode 1 Poincaré wave solution is shown in (e) and (f). Column (i) shows displacements of the two internal interfaces along a west–east section; (ii) displacement of the upper internal interface, with dark lines representing depression and light lines representing elevation; (iii) displacement of the lower internal interface; (iv) velocity vectors in the upper layer; (v) velocity vectors in the middle layer; (vi) velocity vectors in the lower layer. Velocity vectors are normalized by the maximum velocity for each wave and represent the relative contribution to the velocity field in each layer by each wave.

clockwise direction. The dominant feature of the horizontal velocity field measured at Sta. T10 was a 24-h signal that occurred around midday at 10–12 m depth, situated above the metalimnion and flowing toward the south. This velocity signal is consistent with the passage of a progressive internal wave (Fig. 4a,b), with velocities above the interface at the time of the trough flowing in the direction of propagation of the wave. Velocities in this region were thus dominated by the Kelvin wave. The influence of the Kelvin wave in the lake interior is discussed, based on the 1998 ADCP data, in the following discussion on higher vertical mode Poincaré waves.

Vertical mode 1 Poincaré wave: Spectral analysis of integrated potential energy from 1998 (Fig. 5) as well as previous investigations (Serruya 1975) have identified a strong 12-h signal in the isotherm response of the first vertical mode. The theoretical analysis indicates this to be a Poincaré mode of the first horizontal mode, and so in cross section, the wave should appear to be standing (Fig. 4c,d), as observed by Ostrovsky et al. (1996). The wave crest should, however, propagate clockwise around the basin in 12 h. The distance between the Sta. T2 and T9 along the 25-m isobath is 7,300 m, with the length of the 25-m isobath being 35,000 m. The phase of the 12-h wave should progress at 0.81 m s^{-1} and should travel between stations in approximately 2.5 h if the wave propagates clockwise, as the theoretical analysis indicates it will.

In order to demonstrate this clockwise phase progression, 4 d of data from the 1997 experiment at Sta. T2 and T9 are presented in Fig. 8. During this time, the crests of the Kelvin wave and the 12-h wave were in phase, and so the second crest of the 12-h wave occurred during the trough of the 24-h Kelvin wave. The figure shows the clockwise phase progression of the 12-h wave from Sta. T9 to Sta. T2 in 2–3 h when the wind is not acting (i.e., from 0000 to 1200 h). During the action of the wind (i.e., from 1200 to 2400 h), the times are extended, as the forcing does not allow the waves to propagate freely. Figure 8 also shows the anticlockwise phase progression of the Kelvin wave, which was originally demonstrated by Serruya (1975). Associated with the 12-h Poincaré wave should be a strong clockwise component

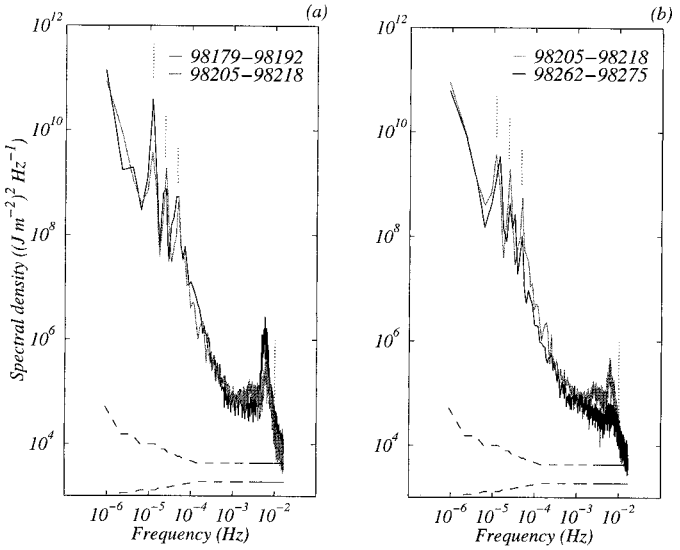

Fig. 5. Power spectra of integrated potential energy. Periods 1 and 2 are shown in (a), and periods 2 and 3 are shown in (b). Dotted vertical lines represent periods of 24, 12, and 6 h and 100 s, from left to right. Spectra have been smoothed in the frequency domain to improve confidence, with confidence at the 95% level shown by the dashed lines.

of the velocity signal, which is demonstrated in the following section.

Vertical mode 2 and vertical mode 3 Poincaré waves: Vertical structure: The magnitude of the vertical mode 1 Kelvin and Poincaré waves makes the identification of a higher vertical mode response using thermistor chain records difficult; therefore, the velocity signal was used. The velocity structure for the first three vertical modes is presented in Fig. 9, with the vertical velocity component *w(z)* and horizontal velocity component *u(z)* calculated based on the average density profile during the first analysis period. A vertical mode 2 response will be characterized by a single peak in the horizontal velocity signal at middepth for typical summer stratification conditions in Lake Kinneret, whereas a vertical mode 3 response will be characterized by two peaks in the horizontal velocity signal close to middepth in opposite directions.

The horizontal velocity field from the ADCPs at Sta. T3 during the 1998 experiment shows a higher vertical mode internal wave response of the water column (Fig. 10). The dominant feature of the velocity field was a strong daily peak that occurred 3–4 h after the onset of the wind, with peak speeds of 27 cm s^{-1} flowing in an east–northeast direction (330°).

The vertical structure of the velocity field can be interpreted as a combination of a vertical mode 2 and vertical mode 3 response. The higher vertical mode response between days 190.5 and 191.5 (Fig. 10) showed a strong vertical mode 3 component, with two peaks present (e.g., at 13 and 18 m depth at day 190.9). It is postulated that the difference in magnitude between the peaks is caused by the presence of the vertical mode 2 wave, as a vertical mode 2 and a vertical mode 3 wave approximately in phase will result in two velocity peaks, with the peak located higher in the water column being the peak of greater magnitude. The vertical mode 3 response appears again between days 191.5 and 192.5, but it is less obvious than it was on the previous day. Day 192.5–193.5 shows a vertical mode 2 component dominating the velocity structure, with only one peak at middepth. The presence of the vertical mode 2 and 3 waves can be made clearer by projecting the current speeds onto an isopycnal coordinate system, as shown in Fig. 11 for the full sampling period of the ADCP station. Velocities on days 186.5–187.5, 189.5–190.5, 190.5–191.5, and 191.5–192.5 were centered around the 24.5°C isotherm, the location of the upper velocity peak for a vertical mode 3 wave, whereas velocities on days 192.5–193.5 and 193.5–194 were centered around the 22°C isotherm, the location of the velocity peak for a vertical mode 2 wave.

Frequency content: The frequency content of the velocity field was determined through rotary spectral analysis (Gonella 1972) of isopycnal velocities (Fig. 12). The velocity at the depth of the 22°C isotherm, the location of the vertical mode 2 eigenfunction peak and the vertical mode 1 eigenfunction minimum (Fig. 9), showed a clockwise-rotating, broad significant peak between 1.04e-5 Hz and 1.49e-5 Hz (18.7–26.7 h). The velocity at the depth of the 24.5°C isotherm, the location of the vertical mode 3 eigenfunction peak, showed a significant peak at a similar frequency as well as at 2.38e-5 Hz (11.7 h), rotating clockwise. The strength of the clockwise-rotating component of the velocity at these two frequencies implies that the oscillations were Poincaré modes (Gill 1982). If the Kelvin wave effect on velocity in the metalimnion was present at Sta. T3, a strong anticlockwise component should have been observed near 24 h for the 24.5°C isotherm. A significant anticlockwise peak was not present, and so we conclude that the effect of the Kelvin wave on velocity in the metalimnion was minor in the lake interior.

Using the spectrum of integrated potential energy to determine the frequency of the higher vertical mode waves is complicated by the effect of the vertical mode 1 Kelvin wave at a similar frequency on the signal. The dispersive nature of Poincaré waves means that they cannot have frequencies lower than the inertial frequency (Csanady 1967; Gill 1982). The Fourier frequency resolution of the velocity signal (Fig. 12) is relatively poor because of the limited record; however, based on the three-layer model, the velocity spectra, and the knowledge that the Poincaré wave must be superinertial, we estimate the period of these higher vertical mode waves as 20 $\pm$ 2 h. The periods of the vertical mode 2 and vertical mode 3 waves are likely to differ by 1–2 h. The third vertical mode period can be estimated by assuming a nonrotating phase speed *c* and solving the circular basin case previously presented. A phase speed of 0.10 m s^{-1} gives a period of 20.0 h. We were unable to separate the vertical mode 2 and vertical mode 3 components from the velocity data, and so we consider them together.

Horizontal structure: Previous investigations of Poincaré waves by Csanady (1967, 1973) have shown that the response to a uniform wind stress favors the first horizontal

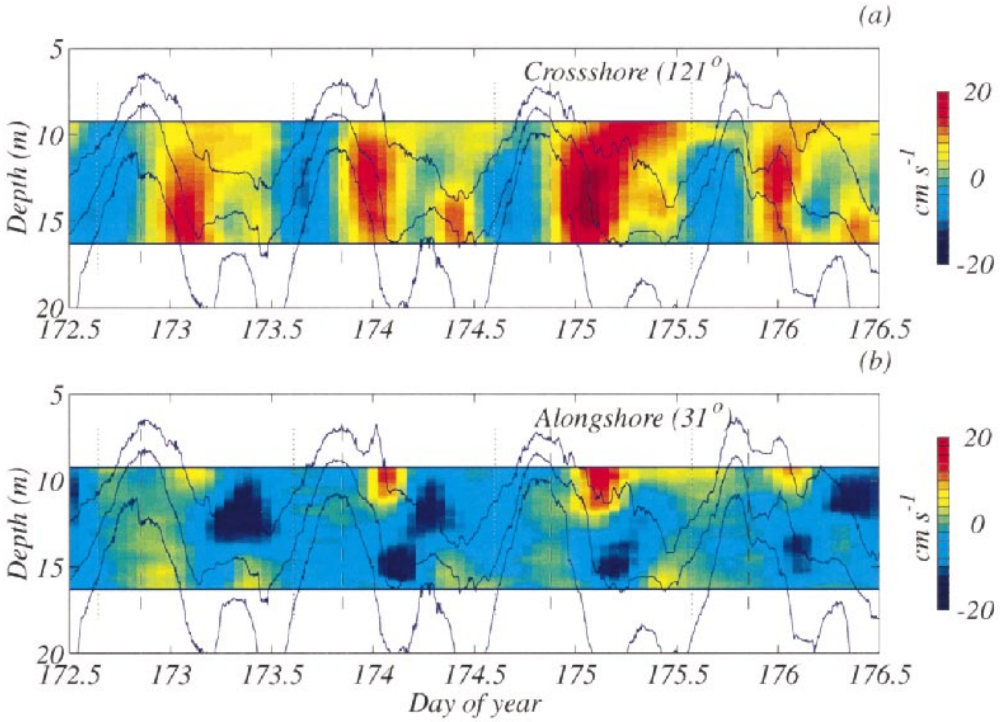

Fig. 6. ADCP record from Sta. T8, 1997: (a) cross-shore velocities, (b) alongshore velocities, with positive defined in the direction indicated. Overlain are displacements of the 18, 22, and 26°C isotherms from Sta. T2, filtered and resampled at 5-min intervals. Dotted vertical lines show the time of onset of the wind, with dashed vertical lines showing the cessation of the wind.

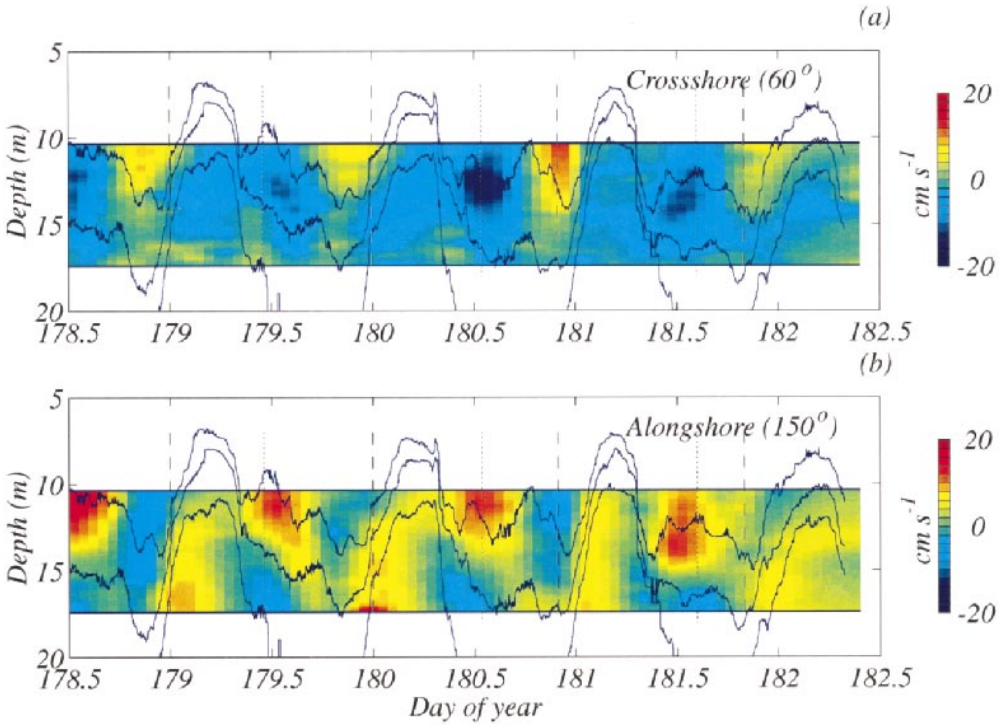

Fig. 7. As for Fig. 6, from Sta. T10, 1997, with isotherms from Sta. T9.

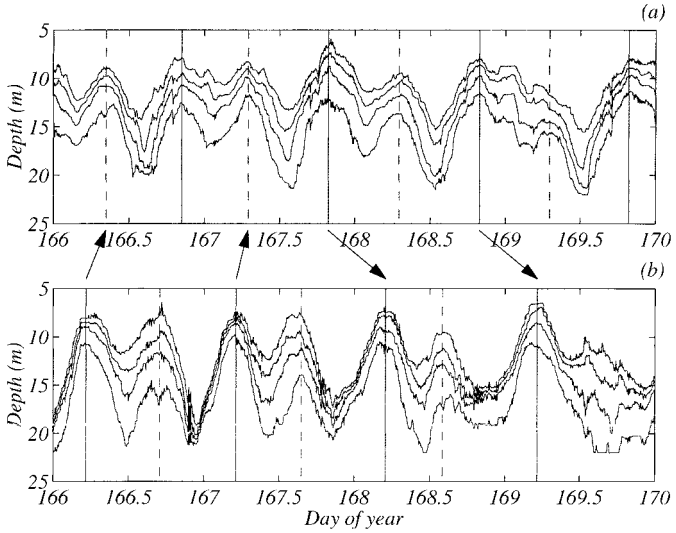

Fig. 8. Isotherm displacements from Sta. T2 (a) and T9 (b) from the 1997 experiment. Crests of the 24-h vertical mode 1 Kelvin wave are indicated with solid vertical lines. Crests of the 12-h vertical mode 1 Poincaré wave are indicated by both dashed and solid vertical lines. Crest locations were chosen by visual inspection of the isotherm record. Upward-facing arrows show the clockwise phase progression of the 12-h Poincaré wave, with downward-facing arrows showing the anticlockwise phase progression of the 24-h Kelvin wave. Only two examples for each wave are highlighted, though the pattern repeats daily.

mode for basins whose width was similar or slightly larger than the internal Rossby radius. This is the case for Lake Kinneret during the period of investigation (*see Table 2 and Fig. 1*), and previous transects of temperature (Ostrovsky et al. 1996) indicate that the higher vertical mode waves are of the first horizontal mode. The horizontal modal structure is also clearly demonstrated by an analysis of the spatial velocity field. A transect, cycling from T4 through to T2 (*see Fig. 1*), was completed four times from 1330 h on day 98187 until 0630 h on day 98188 using the Portable Flux Profiler (PFP) (Imberger and Head 1994). Several microstructure profiles of temperature and the three components of velocity were made at each station during each cycle. The microstructure measurements of velocity were corrected for the motion of the probe (Saggio and Imberger in prep.) to give the actual water velocities. Profiles of temperature, speed, and direction at Sta. T3 and T4 for the final pass are presented in Fig. 13. Data from Sta. T2 were not included, as the metalimnion intercepted the bottom boundary at this location. The time difference between the first and last profile was 60 min, approximately T/20, allowing the ''frozen flow'' approximation to be applied. Mortimer (1974) demonstrated that for Poincaré waves of higher horizontal modes, the velocities in adjacent cells were exactly opposite, with the maximum velocity occurring in the cell center and decreasing toward the cell boundary. The peak in the profiles of speed, centered around 16 m depth, represent the higher vertical mode response of the water column. From Fig. 13 we note that the speed decreased from T4 to T3 and that the flow direction associated with the higher vertical mode waves was similar at both stations. The higher vertical mode response of the

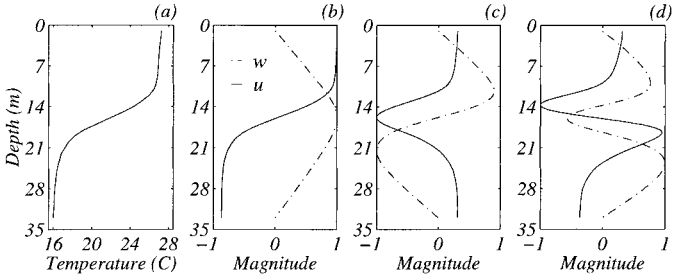

Fig. 9. Vertical modal structure: (a) background stratification during analysis period 1; (b) vertical mode 1 eigenfunctions for horizontal velocity *u* and vertical velocity *w*, for the stratification in (a); (c) vertical mode 2 eigenfunctions; (d) vertical mode 3 eigenfunctions.

water column is therefore interpreted as being horizontal mode 1 (Fig. 4e,f), with the cell center located in the vicinity of Sta. T4.

Evolution of the basin-scale internal wave field

Evolution of the vertical mode 1 Kelvin and Poincaré waves—The changing stratification and wind forcing had a major effect on the structure of the internal wave field (Figs. 3, 5) during the extended deployment of 1998. To trace the evolution of the vertical mode 1 components of the basin-scale response, the vertical mode 1 Kelvin and Poincaré waves were identified by features in the integrated potential energy time series with periods of 24 h (1.1e-5 Hz) and 12 h (2.3e-5 Hz), respectively. The contribution of higher vertical mode waves to the integrated potential energy signal at these frequencies has already been shown to be small. During the second deployment period, the period of the Kelvin wave decreased to approximately 20 h (1.4e-5 Hz) (Fig. 5b), shifting from a subinertial to a superinertial frequency, in keeping with the analytical result for the elliptic basin case previously presented. The change in frequency was attributed to the less dominant effect of the wind and the slightly increased stratification, and so we identified the Kelvin wave evolution during the second deployment period (98251–98287) by features in the integrated potential energy time series at 1.4e-5 Hz. We discuss the amplitude and phase evolution of the vertical mode 1 basin-scale waves and then investigate generation mechanisms based on data from the 1998 experiment.

Amplitude evolution: The bulk features of the amplitude evolution of the vertical mode 1 Kelvin and Poincaré waves over the three analysis periods was obtained from the peaks in the power spectra of integrated potential energy in Fig. 5. The potential energy at 24 h decreased substantially between the first and second periods and increased at 12 h. Despite the fact that the momentum input from the wind decreased substantially between the second and third periods (u_*^2; Table 2), the amount of energy at 24 h remained constant, whereas the energy at 12 h decreased.

The amplitude evolution of these Kelvin and Poincaré waves was investigated with greater temporal resolution using two independent methods: the continuous wavelet trans-

form of the integrated potential energy time series and the eigenfunction-fitting technique. The continuous wavelet transform returns real coefficients $c(\omega, t)$, from which we determined the time of day at which maxima and minima in the wavelet transform coefficients occurred on a daily basis. These corresponded to crests and troughs of vertical mode 1 internal waves. The eigenfunction-fitting technique returns amplitudes A and phases ϕ directly (Eq. 2).

The amplitude evolution was investigated by making a two-layer approximation to the stratification and by then finding the displacement (or ''equivalent amplitude'') of the internal interface required to give the same integrated potential energy as the waves in the continuous stratification. The integrated potential energy signal for a two-layer system is

$$PE(t) = \frac{g}{2}[\rho_2(h_2 + \eta)^2 + \rho_1(h_1 + h_2)^2 - \rho_1(h_2 + \eta)^2], \quad (13)$$

where $\eta = \eta_0 \sin \omega t$, and the subscripts 1 and 2 refer to the upper and lower layers, respectively, with η representing the amplitude of interface displacement about its equilibrium state. The integrated potential energy due to a wave involves only those terms containing η:

$$PE_{wave}(t) = \frac{g}{2}[2\eta h_2(\rho_2 - \rho_1) + \eta^2(\rho_2 - \rho_1)]. \quad (14)$$

Using the continuous wavelet transform, the displacement η_0 of the internal interface of the two-layer system required to match the transform coefficients for the field-integrated potential energy signal and the two-layer system (Eq. 14) was determined. For the eigenfunction-fitting technique, the maximum integrated potential energy due to each wave was calculated by determining the amplitude A, substituting Eq. 2 into Eq. 1, and integrating. The equivalent amplitude in a two-layer system was determined by equating the value obtained with Eq. 14, with η_0 the independent variable. All calculations were made on a daily basis.

The amplitude evolution of the vertical mode 1 Kelvin and Poincaré waves during 1998 is shown in Fig. 14. For the first deployment period, the Kelvin wave amplitude (Fig. 14a) increased dramatically on day 182, decreasing after days 185 and 200. By the end of the deployment period, the amplitude was approximately one-half the initial value. Similar trends were identified through both the continuous wavelet transform and eigenfunction fitting, with the result also supported by visual inspection of the temperature record in Fig. 3b. The evolution of the 12-h vertical mode 1 Poincaré wave (Fig. 14c) varied little over the period and did not follow the same trend as was noted for the Kelvin wave. Some features are linked, however, with strong signals for both waves between days 98182 and 98185. The dramatic drop in Kelvin wave energy after day 98200 was also reflected in the Poincaré wave signal, though the Poincaré wave amplitude recovered to its initial amplitude. The evolution of these waves during the second deployment period (Fig. 14b,d) follows the observations made from the thermistor chain data (Fig. 3d), with the 12-h Poincaré wave signal being strong initially and with the Kelvin wave signal increasing after day 98266.

Phase evolution: The continuous wavelet transform of the integrated potential energy time series was used to determine the phase evolution of these waves during the 1998 experiment. The arrival times of the crests and troughs of the Kelvin and 12-h Poincaré waves at Sta. T3 (Fig. 15) were determined by finding the times at which crests and troughs in the wavelet transform coefficient series occurred. The crests of the 12-h Poincaré wave occurred around 0800 and 1200 h over both deployment periods, whereas the Kelvin wave displayed a progressive positive phase shift during the first deployment period. This is particularly noticeable after day 198 (17 Jul), which coincided with the decrease in Kelvin wave amplitude (Fig. 14). However, the overall positive phase shift that we observed was most likely due to the Kelvin wave period being slightly less than 24 h. During the second deployment period (Fig. 15b), the Kelvin wave showed a continuous positive phase shift because the period of the wave was less than 24 h. The momentum input during this time was quite variable in magnitude and time of onset compared to those of the first deployment period (Fig. 3a).

The observations of a clear 12-h signal in the first analysis period and of broader crests during the second analysis period (*see Fig. 3b,c*) were thus attributable to the change in phase of the Kelvin wave and the 12-h Poincaré wave. For the first analysis period (day 179–192), the crest and trough of the Kelvin wave were in phase with the crests of the 12-h Poincaré wave, whereas for the second analysis period (day 205–218), they were in phase with the troughs of the 12-h Poincaré wave.

Kelvin wave generation: Consideration of only the momentum input by the wind is insufficient to explain the observed decrease in energy in the Kelvin wave during the first deployment period, as the wind field is relatively similar (Fig. 3). Clearly, the steady-state Lake number parameterization presented previously was inadequate in explaining the energy decrease. The periodic nature of the wind forcing and Kelvin wave response indicates that wave resonance was important.

In order to investigate the effect of the relative phase of the wind and the Kelvin wave, we first solve the normal mode equations (Csanady 1982; Monismith 1985) for a two-layer stratification. The internal interface deflection is

$$d = \frac{4}{L}\left(1 - 2\frac{x}{L}\right)\frac{h_2}{h_1 + h_2}\int_0^{T/4}\int_0^{t'} u_*^2 \, dt' \, dt, \quad (15)$$

where h_1 and h_2 are the layer depths and d the interface deflection at time $T/4$ and position x/L. The origin of x is at the upwind end. For a constant wind stress,

$$d = \left(1 - 2\frac{x}{L}\right)\frac{h_2}{h_1 + h_2}\frac{L}{2Ri}, \quad (16)$$

where Ri is defined previously. This reduces to the result of Stevens and Lawrence (1997) for a thin surface layer. As an indicator of the forced response of the lake, we model the effect of the forcing by assuming the interface response to be described by a simple spring-mass system equation, where the forcing is applied impulsively at t_0. An impulsive wind force was used, as the wind duration was typically one-

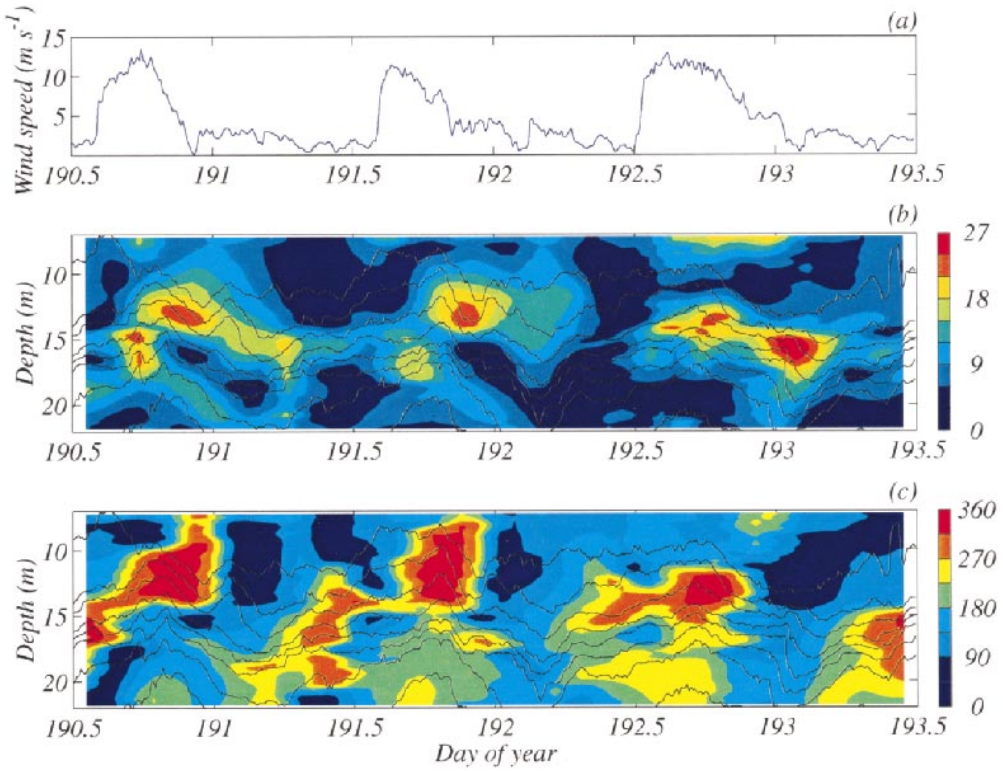

Fig. 10. ADCP record from Sta. T3, 1998: (a) 10-min average of the wind speed corrected to 10 m above the water surface; (b) resolved horizontal speed in cm s^{-1}, superimposed on the record of isotherm displacement with the top isotherm 27°C and a contour interval of 1.5°C; (c) current direction as per oceanographic convention, with isotherms as for (b).

quarter of the Kelvin wave period. The solution of the system takes the form

$$z = Z_0 \sin\, \omega t + dH(t - t_0)\sin\, \omega(t - t_0), \qquad (17)$$

where Z_0 is the initial amplitude and $H(t - t_0)$ represents the Heaviside step function.

For the system described above, the relative phase of the wind impulse and the wave becomes less important as the ratio of d to Z_0 increases, as the momentum input overrides the initial condition; the phase band in which amplitude decreases ($z_{max} < Z_0$) can occur becomes narrower (Fig. 16). To estimate the importance of relative phase of the wind and the Kelvin wave in Lake Kinneret, d/Z_0 was estimated using the parameters in Table 2, with $x/L = 0.43$ at Sta. T3. In all cases, the ratio is less than unity (Table 4), and so the relative phase of the wind and the Kelvin wave plays an important role in determining the amplitude of the Kelvin wave.

The magnitude, duration, and phase of the wind to the

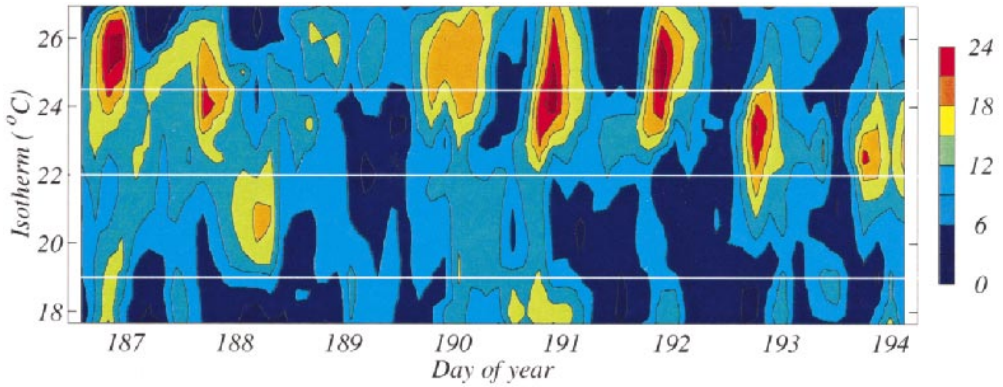

Fig. 11. ADCP record from Sta. T3 in an isopycnal coordinate system, with horizontal speed in cm s^{-1} for isotherms between 18 and 27°C. All mapping was based on linear interpolation at 0.5°C intervals. Horizontal lines represent 24.5, 22, and 19°C—the location of the peak velocities for the mode 3, mode 2, and mode 3 waves, respectively—derived from the eigenvalue problem.

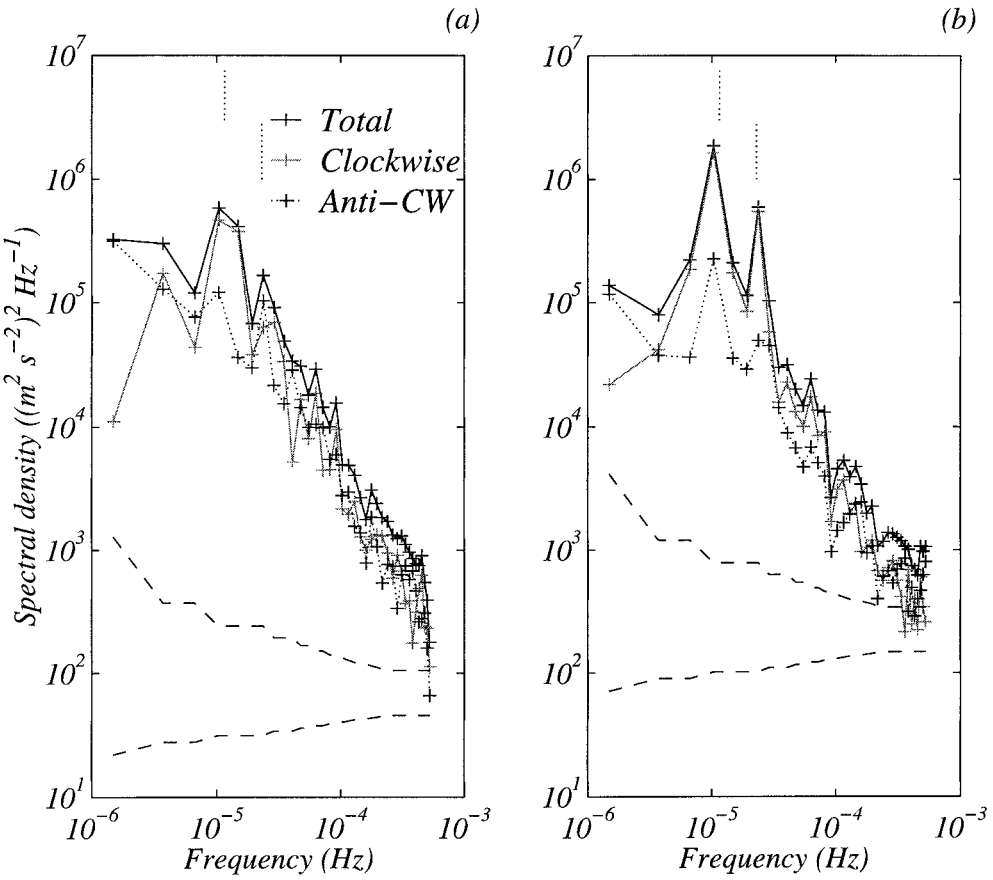

Fig. 12. Rotary power spectra of isopycnal speed, decomposed into clockwise and anticlockwise rotating components: (a) the 22°C isotherm; (b) the 24.5°C isotherm. Vertical dashed lines from left to right are positioned at 24 and 12 h, respectively. Crosses show the Fourier frequency discretization, with spectra smoothed in the frequency domain to improve confidence and confidence at the 95% level shown by the dashed lines.

Kelvin wave, as well as the Kelvin wave amplitude, are presented in Fig. 17. The largest Kelvin wave amplitudes (98181–98184) were associated with large momentum input and a relative phase of close to zero, the most favorable condition for resonant amplification (Fig. 16). Although the momentum input on day 98193 was similar to that on 98182, the Kelvin wave response was smaller because the relative phase was less favorable for resonant amplification. After day 98200, there was a dramatic phase shift because wind onset was 3 h ($T/8$) later than it had been the previous day (Fig. 15a). Subsequent wind events did not result in Kelvin wave amplitudes that were as large as those prior to day 98200 because the relative phase ($\sim T/3$) was unfavorable for resonant amplification. The behavior of the Kelvin wave during the second deployment period of 1998 can also be explained by this model. The large wind events from 98260 to 98263 had little effect on the Kelvin wave amplitude, except on day 98263, when the relative phase was low. The slight increase in Kelvin wave energy observed after day 98267 was attributed to a small relative phase difference on both days 98266 and 9826—a difference of approximately $T/10$—combined with relatively large wind events for the period.

Poincaré wave generation: The magnitude, duration, and relative phase of the wind, as well as the Poincaré wave amplitude, are presented in Fig. 18. We do not use the impulse model in describing the evolution of this wave as the wind duration approaches $T/2$, but we do include the relative phase in the figure for consistency with Fig. 17. The amplitude of the Poincaré wave follows the evolution of the momentum input closely, with both wind and wave amplitudes being greatest during the first deployment period and lower during the second deployment period. The highest Poincaré wave amplitudes were associated with large wind events during both periods (e.g., 98182, 98189, 98207, 98262, and 98266). Days of little momentum input by the wind (e.g., 98186, 98200, and 98257) coincided with smaller amplitudes of the wave.

Despite the fact that the momentum input decreased dramatically between the two deployment periods (Fig. 18), the values for energy in the Poincaré wave remained relatively similar. The increased efficiency of energy transfer from the wind to the Poincaré wave during the second period may have been due to the changing stratification altering the partitioning of energy into the vertical mode 1 and 2 responses (Stevens and Lawrence 1997). This seems unlikely to be the

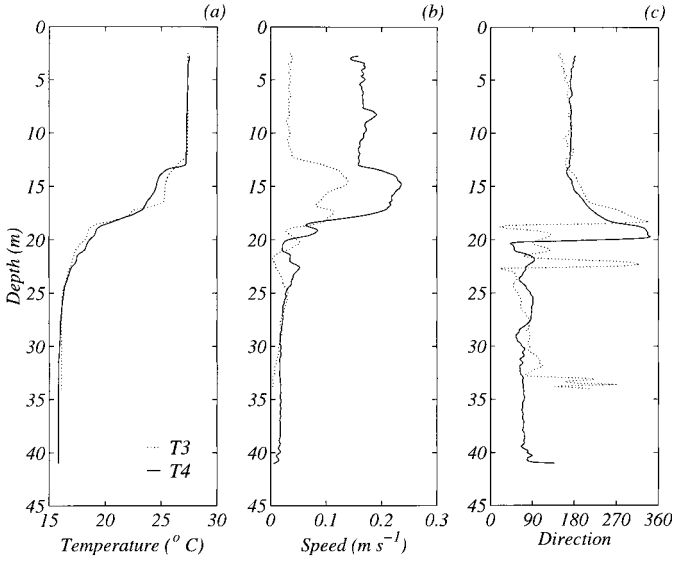

Fig. 13. Averaged profiles of (a) temperature, (b) speed, and (c) direction at Sta. T3 and T4. Profiles were collected with the PFP at 0441 and 0448 h at Sta. T4 and at 0535 and 0544 h at Sta. T3 (on day 98188). Profiles from each station were smoothed over 5 cm and averaged together.

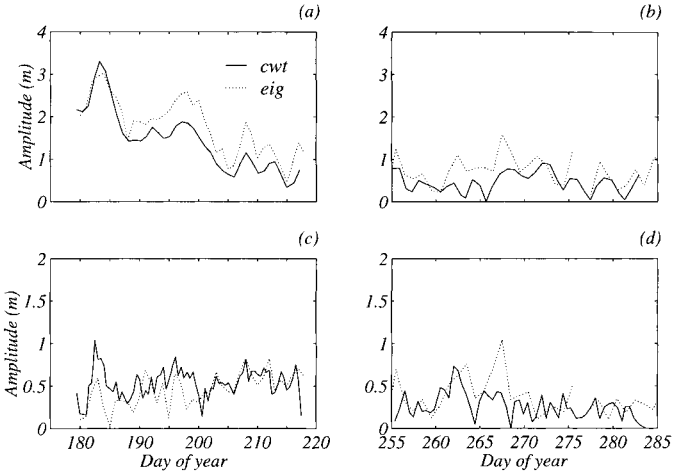

Fig. 14. Amplitude evolution of the vertical mode 1 Kelvin (a, b) and Poincaré waves (c, d) during the 1998 experiment. Equivalent amplitudes determined from the continuous wavelet transform of the integrated potential energy signal at 24 h are shown by the solid line, with equivalent amplitudes derived from the eigenfunction-fitting technique shown by the dotted lines. Layer depths of 11 and 13 m and temperatures of 28 and 20°C were chosen for the two-layer approximation.

most important factor, as the stratification changed only slightly between the second and third analysis period compared to the momentum input (Fig. 2, Table 2). The dynamics of the epilimnion was more likely responsible for the observed increased efficiency, as the lake was cooling during the second deployment period (Fig. 3d), and so the epilimnion was less stratified at this time than it had been during the first deployment period (Fig. 2). The partitioning of energy imparted by the wind between the baroclinic response, the surface-layer circulation, and dissipative losses is likely to have been vastly different (Stevens and Imberger 1996).

Evolution of the vertical mode 2 and 3 Poincaré waves—Investigation of the evolution of the vertical mode 2 and 3 Poincaré waves was difficult because of the effect of the dominant vertical mode 1 Kelvin wave on the temperature signal at a similar period. Visual inspection of the temperature record (Fig. 3) and the integrated potential energy signal (Fig. 5) shows that the internal wave field was most energetic during the first analysis period and least energetic during the third analysis period of 1998. We expect to find a similar pattern in the evolution of the vertical mode 2 and 3 Poincaré waves, based on the Wedderburn number (Table 2).

In order to estimate the importance of relative phase of the wind and the higher mode Poincaré waves in Lake Kinneret, we assume a three-layer stratification and solve the normal mode problem as for the two-layer case. The internal deflections are

$$d_{mi} = (-1)^i \frac{4}{L}\left(1 - 2\frac{x}{L}\right)\frac{A_{(m,2i-3)}a_{(m,1)}}{|a|}\int_0^{T_m/4}\int_0^{t'} u_*^2\, dt'\, dt. \quad (18)$$

For a constant wind stress,

$$d_{mi} = (-1)^i \frac{A_{(m,2i-3)}a_{(m,1)}}{|a|}\left(1 - 2\frac{x}{L}\right)\frac{L}{2Ri_m}, \quad (19)$$

where $Ri_m = c_m^2/u_*^2$. The matrix a is given in Csanady (1982), A_{jk} is the cofactor of a_{jk}, and $|a|$ the determinant. The normal mode approximation to the linear equations gives solutions to the individual modes on different interfaces separately, and so the solution for an impulsively applied wind force takes the form

$$z_i = Z_{2i}\sin\,\omega_2 t + Z_{3i}\sin\,\omega_3 t + d_{2i}H(t - t_0)\sin\,\omega_2(t - t_0) + d_{3i}H(t - t_0)\sin\,\omega_3(t - t_0) \quad (20)$$

where $i = 2$ for the first internal interface and $i = 3$ for the second internal interface. The free solutions are described by $Z_{mi}\sin\,\omega_m t$, where m is the modal index ($m = 2$ for the first baroclinic mode) and i the interface index. We assume there is no phase difference between the free solutions, as they are both forced initially by the same wind event.

For the three-layer stratification in Table 3 for analysis period 1, we find $d_{22} = 0.32$ m, $d_{32} = 0.07$ m, $d_{23} = 0.40$ m, and $d_{33} = -0.40$ m. Initial amplitudes Z_{mi} are difficult to determine, but we expect d_{mi}/Z_{mi} to be O(1). The effect of the phase on the waves is the same as that presented in Fig. 16. The phase difference will vary greatly on a daily basis as a result of the 4-h difference in period of wave and the return period of the wind forcing. This is likely to result in widely varying magnitudes of the higher vertical mode waves on a daily basis.

To identify further features of the evolution of the vertical mode 2 and 3 Poincaré wave, we applied the eigenfunction-fitting technique outlined previously. The waves chosen to approximate the data were the 24-h Kelvin wave, the 20-h vertical mode 2 and vertical mode 3 Poincaré waves, and the vertical mode 1 12-h Poincaré wave. The mean values

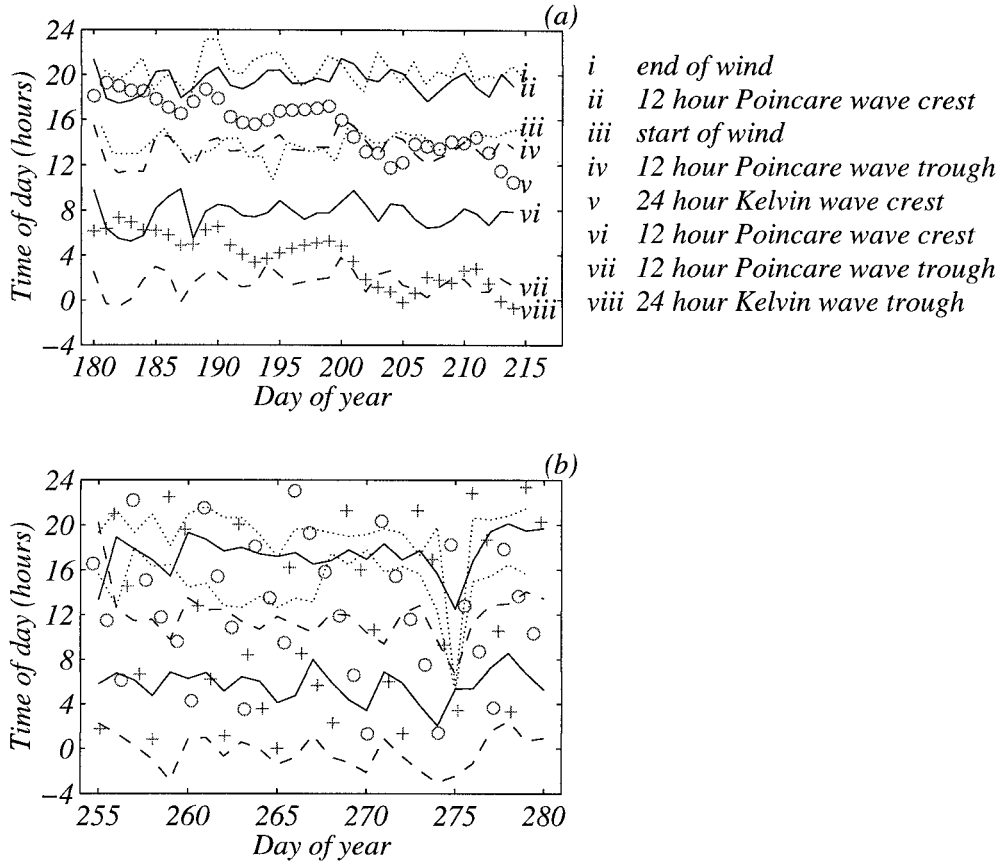

Fig. 15. Basin-scale wave phase relationship for the 1998 experiment, calculated from the arrival times of crests and troughs of the 24- and 12-h components in the signal of integrated potential energy, computed via wavelet transforms, is presented in Fig. 15. Lines represent the following: (i) cessation of daily westerly wind event; (ii) 12-h Poincaré wave crest; (iii) onset of daily westerly wind event; (iv) 12-h Poincaré wave trough; (v) 24-h Kelvin wave crest; (vi) 12-h Poincaré wave crest; (vii) 12-h Poincaré wave trough; (viii) 24-h Kelvin wave trough—all for deployment periods 1 and 2.

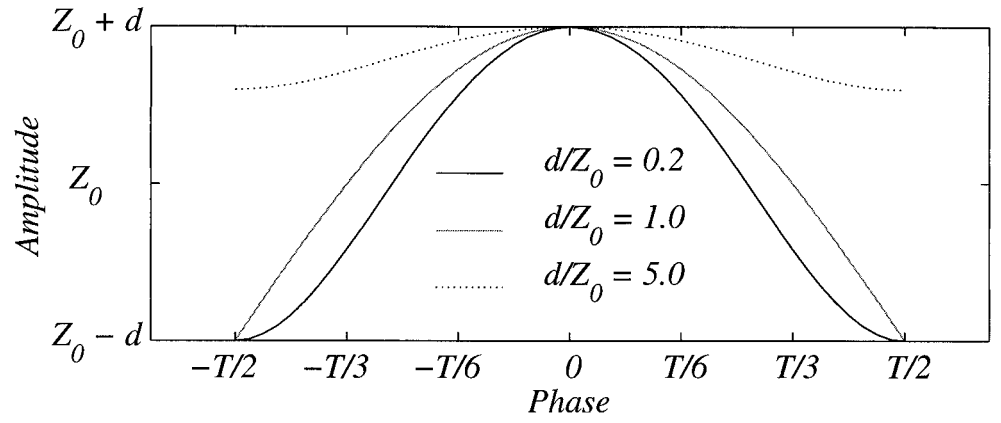

Fig. 16. Impulse model amplitude/phase diagram, showing the relationship between the change in amplitude and the relative phase of the impulsive forcing for several ratios of amplitude prior to onset Z_0 to interface deflection due to the wind event d. A relative phase of zero is defined as the impulsive force being applied as the wave passes through zero from trough to crest and is most favorable for resonant amplification.

Table 4. Impulse model amplitudes for Lake Kinneret during 1998, with d = the deflection due to the wind; Z_0 = the initial wave amplitude; and ϕ_c = the critical phase. Wind events occurring impulsively $\phi_c T$ h before or after the zero crossing of the wave from trough to crest will cause a decrease in amplitude. T is the period of the wave under investigation, in the case 24 h.

Period	d (m)	z_0 (m)	d/Z_0	ϕ_c	$\phi_c T$ (h)
1	0.6	2	0.3	$\pm 0.28T$	± 6.6
2	0.5	1	0.5	$\pm 0.29T$	± 7.0
3	0.03	0.5	0.06	$\pm 0.25T$	± 6.1

of the magnitudes A_m for the four waves during the three periods of analysis are presented in Fig. 19.

The mean behavior of the vertical mode 2 and vertical mode 3 Poincaré waves was similar during each period. Both were at a maximum during the first period and at a minimum during the third period, which can be seen by careful inspection of Fig. 3. The evolution of the higher vertical mode waves follows a similar trend to the evolution of the Kelvin wave rather than the Wedderburn number (Table 2), indicating that prior motion of the water column has an effect on the generation of these waves. The size of the spread in the magnitudes of the vertical mode 2 and 3 waves within each analysis period indicates that the waves were not consistently generated despite the regularity of the wind forcing. This spread follows the three-layer resonance model results, as the waves will change phase relative to the wind by $T/5$ each day because of the difference in periods, which in turn affects the energy in the waves.

Conclusions

Analysis of thermistor chain and ADCP data in Lake Kinneret during 1997 and 1998 revealed an energetic basin-scale internal wave field, which was forced daily by a strong sea breeze of up to 15 m s^{-1}. As well as observing the Kelvin wave previously identified in the lake, basin-scale horizontal mode 1 Poincaré waves of vertical modes 1, 2, and 3 were demonstrated to exist. The features of the measured basin-scale internal wave response were similar to those predicted by the three-layer case (Table 5). The vertical mode 1 components of the internal wave field matched the periods of the three-layer model particularly well, with the vertical mode 2 prediction being less accurate. This was attributed to the sensitivity of vertical mode 2 waves to the structure of the metalimnion (Monismith 1985) (and hence, the three-layer approximation made). The field response was also shown to have a significant vertical mode 3 component, which was not captured by the three-layer approximation.

The Kelvin wave induced alongshore velocities in the nearshore regions, although in the upwind nearshore region

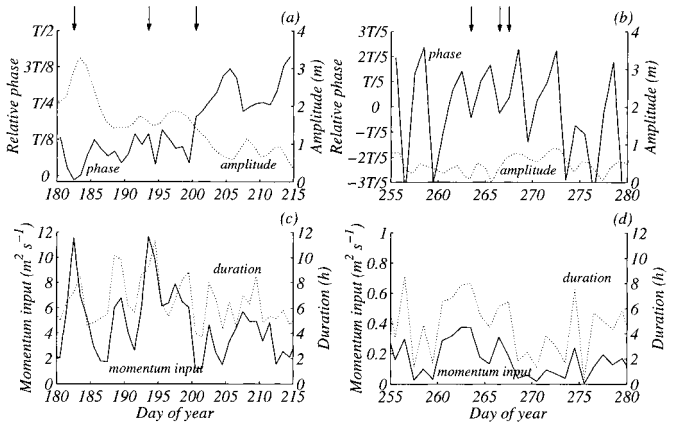

Fig. 17. Wind characteristics and Kelvin wave amplitude during the 1998 experiment. Kelvin wave amplitudes are those derived from the continuous wavelet transform, as in Fig. 14. For each panel, left-hand axes are for the solid line and right-hand axes for the dotted line. Panels (a) and (b) show relative phase (solid) and Kelvin wave amplitude (dotted) for both deployment periods of 1998. Panels (c) and (d) show total momentum input for a wind event (solid) and wind event duration (dotted) for both deployment periods of 1998. Arrows point to days discussed in the text.

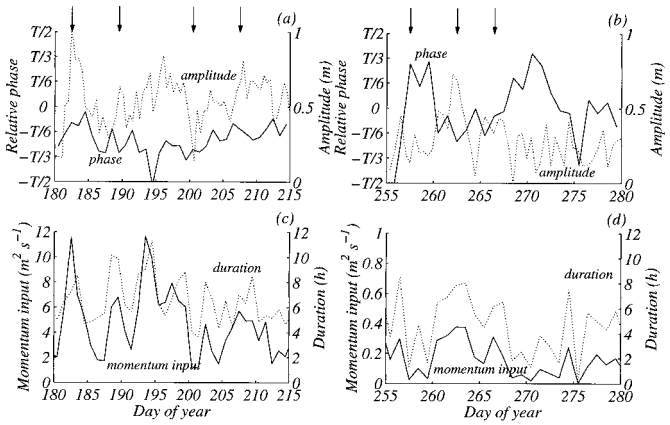

Fig. 18. As for Fig. 17, but for the 12-h Poincaré wave.

The Kelvin wave induced alongshore velocities in the nearshore regions, although in the upwind nearshore region

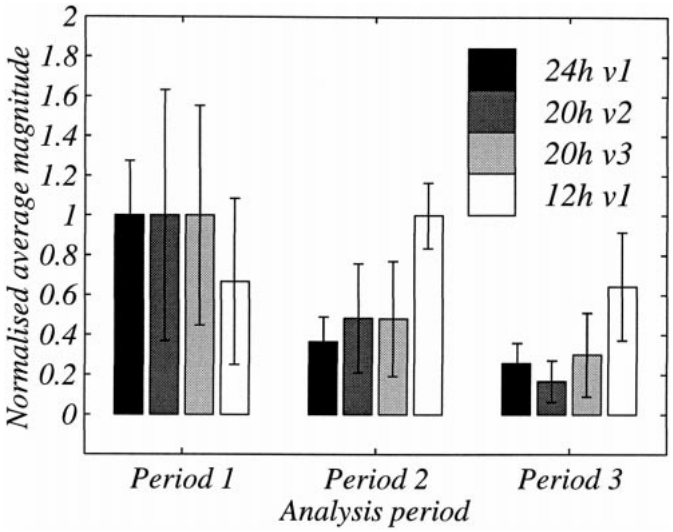

Fig. 19. Normalized mean magnitude of coefficients A_m returned by the eigenfunction fitting for analysis periods 1–3 for the 24-h Kelvin wave, 20-h vertical mode 2 and 3 Poincaré waves, and 12-h vertical mode 1 Poincaré waves, respectively (dark to light shading). Vertical bars represent one standard deviation from the mean. Coefficients are normalized to show relative evolution.

Table 5. Basin-scale internal wave summary.

Period (h) Field	Period (h) Three-layer model	Vertical mode	Horizontal mode	Wave type
24	22.5	One	One	Kelvin
12	12.2	One	One	Poincaré
20±2	17.5	Two	One	Poincaré
20±2	—	Three	One	Poincaré

of the lake, velocities were dominated by the forced response to the wind. Horizontal motion near the boundaries is thus due to either the forced response to the wind, and is cross-shore (Sta. T8), or to the free propagation of the Kelvin wave in the alongshore direction (Sta. T10). Horizontal motion in the interior will be dominated by the Poincaré waves. The latter effect is clearly shown by the strong clockwise component of the velocity field at Sta. T3 (Fig. 12), where the velocity field at this station was dominated by Poincaré motion. The interaction between the vertical mode 2 and vertical mode 3 Poincaré waves (with periods of approximately 20 h) determined the velocity response in the metalimnion in the lake interior.

The phase relationship between the 24-h period Kelvin wave and the 12-h period vertical mode 1 Poincaré wave was found to determine the lowest mode isotherm response. For the 1998 deployment, greater momentum input resulted in greater energy in the 12-h vertical mode 1 Poincaré wave. The energy in the wave remained comparable over widely varying conditions of wind forcing and was therefore relatively insensitive to the applied wind stress.

The energy in the higher vertical mode Poincaré waves was found to vary greatly on both daily and seasonal timescales. The daily variability was postulated to be due to the difference in period of the waves and the return period of the wind forcing, resulting in the waves drifting in and out of phase with the wind. The seasonal variability followed the evolution of the Kelvin wave rather than a steady-state Wedderburn-number parameterization, indicating that the residual motion in the water column had a major effect on the generation of these waves.

The periodic nature of the wind forcing was found to play a major role in the propagation of the Kelvin wave, magnifying and repressing the wave depending on the relative wind–wave phase. The resonant and antiresonant interaction with the wind forcing of similar period has significant implications for the circulation pattern in the lake. Ou and Bennett (1979) showed that the mean anticlockwise circulation observed by Serruya (1975) below the thermocline during summer was induced by the nonlinear interaction of bottom stress and the Kelvin wave, indicating that the absence of the Kelvin wave would result in no mean anticlockwise circulation. Serruya (1975) reported periods of little mean circulation or of occasional clockwise circulation when the wind was below 3 m s^{-1} and when the water column was stratified. An explanation for these observations, based on the present data, in particular on observations made during the second deployment period of 1998 (98251–98287), is that the Kelvin wave response was damped and the Poincaré wave responses dominated, resulting in the weak circulation observed. The results indicate that hydrodynamic models must be able to accurately reproduce the generation and propagation characteristics of the waves, as the interplay between the different waves and the wind forcing determines the dynamics of the system.

References

AMOROCHO, J., AND J. J. DEVRIES. 1980. A new evaluation of the wind stress coefficient over water surfaces. J. Geophys. Res. **85:** 433–442.

BUGNON, F. J., AND I. A. WHITEHOUSE. 1991. Acoustic Doppler current meter. IEEE J. Oceanic Eng. **16:** 420–426.

CSANADY, G. T. 1967. Large-scale motion in the Great Lakes. J. Geophys. Res. **72:** 4151–4162.

———. 1973. Transverse internal seiches in large oblong lakes and marginal seas. J. Phys. Oceanogr. **3:** 439–447.

———. 1982. On the structure of transient upwelling events. J. Phys. Oceanogr. **12:** 84–96.

GARRETT, C., AND W. MUNK. 1979. Internal waves in the ocean. Ann. Rev. Fluid Mech. **11:** 339–369.

GILL, A. E. 1982. Atmosphere–ocean dynamics. Academic Press.

GOLDSTEIN, S. 1929. Tidal motion in rotating elliptic basins of constant depth. M. Not. R. Astronom. Soc. (Geophys. Suppl.). **2:** 213–231.

GONELLA, J. 1972. A rotary-component method for analyzing meteorological and oceanographic vector time series. Deep-Sea Res. **19:** 833–846.

IMBERGER, J., AND R. HEAD. 1994. Measurement of turbulent properties in a natural system. Proceedings Fundamentals and Advancements in Hydraulic Measurements and Experimentation. ASCE.

IVEY, G. N., AND R. I. NOKES. 1989. Mixing driven by the breaking of internal waves against sloping boundaries. J. Fluid Mech. **204:** 479–500.

KAISER, G. 1994. A friendly guide to wavelets. Birkhauser.

LAMB, H. 1932. Hydrodynamics, 6th ed. Dover.

LEBLOND, P. H., AND L. A. MYSAK. 1978. Waves in the ocean. Elsevier.

LEMCKERT, C., AND J. IMBERGER. 1998. Turbulent benthic boundary layer mixing events in fresh water lakes, p. 503–516. *In* J. Imberger [ed.], Physical processes in lakes and oceans. Coastal and Estuarine Studies. AGU.

LEMMIN, U. 1987. The structure and dynamics of internal waves in Baldeggersee. Limnol. Oceanogr. **32:** 43–61.

MICHALLET, H., AND G. N. IVEY. 1999. Experiments on mixing due to internal solitary waves breaking on uniform slopes. J. Geophys. Res. **104:** 13467–13478.

MONISMITH, S. G. 1985. Wind-forced motions in stratified lakes and their effect on mixed-layer shear. Limnol. Oceanogr. **30:** 771–783.

———. 1986. An experimental study of the upwelling response of stratified reservoirs to surface shear stress. J. Fluid Mech. **171:** 407–441.

MORTIMER, C. H. 1974. Lake hydrodynamics. Mitt. Int. Ver. Limnol. **20:** 124–197.

MOUM, J. N., D. HEBERT, C. A. PAULSON, AND D. R. CALDWELL. 1992. Turbulence and internal waves at the equator: Part 1—statistics from towed thermistors and a microstructure profiler. J. Phys. Oceanogr. **22:** 1330–1345.

MYSAK, L. A., G. SALVADÉ, K. HUTTER, AND T. SCHEIWILLER. 1985. Topographic waves in a stratified elliptical basin, with

application to the Lake of Lugano. Phil. Trans. R. Soc. Lond. **A316:** 1–55.

NEUMANN, J., AND G. STANHILL. 1978. The general meteorological background, p. 49–58. *In* S. Serruya [ed.], Lake Kinneret. Dr. W. Junk.

NISHRI, A., J. IMBERGER, W. ECKERT, I. OSTROVKSY, AND Y. GEIFMAN. 2000. The physical regime and the respective biogeochemical processes in lower water mass of Lake Kinneret. Limnol. Oceanogr. **45:** 972–981.

OSTROVSKY, I., Y. Z. YACOBI, P. WALLINE, AND I. KALIKHMAN. 1996. Seiche-induced mixing: Its impact on lake productivity. Limnol. Oceanogr. **41:** 323–332.

OU, H. W., AND J. R. BENNETT. 1979. A theory of the mean flow driven by long internal waves in a rotating basin, with application to Lake Kinneret. J. Phys. Oceanogr. **9:** 1112–1125.

PHILLIPS, O. M. 1977. The dynamics of the upper ocean, 2nd ed. Cambridge.

ROGET, E., G. SALVADE, F. ZAMBONI, AND J. E. LLEBOT. 1993. Internal waves in a small lake with a thick metalimnion. Verh. Int. Ver. Limnol. **25:** 91–99.

SAGGIO, A., AND J. IMBERGER. 1998. Internal wave weather in a stratified lake. Limnol. Oceanogr. **43:** 1780–1795.

SERRUYA, S. 1975. Wind, water temperature and motions in Lake Kinneret: General pattern. Verh. Int. Ver. Limnol. **19:** 73–87.

STEVENS, C. L., AND J. IMBERGER. 1996. The initial response of a stratified lake to a surface shear stress. J. Fluid Mech. **312:** 39–66.

———, AND G. A. LAWRENCE. 1997. Estimation of wind-forced internal seiche amplitudes in lakes and reservoirs, with data from British Columbia Canada. Aquat. Sci. **59:** 115–134.

STOCKER, T., AND K. HUTTER. 1987. Topographic waves in channels and lakes on the f-plane. Lecture notes on coastal and estuarine studies, v. 21. Springer-Verlag.

THOMSON, SIR W. (LORD KELVIN). 1879. On gravitational oscillations of rotating water. Proc. R. Soc. Edinb. **10:** 92–100.

THORPE, S. A., AND R. JIANG. 1998. Estimating internal waves and diapycnal mixing from conventional mooring data in a lake. Limnol. Oceanogr. **43:** 936–945.

———, J. M. KEEN, R. JIANG, AND U. LEMMIN. 1996. High-frequency internal waves in Lake Geneva. Phil. Trans. R. Soc. Lond. A **354:** 237–257.

WEBB, A. J., AND S. POND. 1986. A modal decomposition of the internal tide in a deep, strongly stratified inlet: Knight Inlet British Columbia. J. Geophys. Res. **91:** 9721–9738.

WIEGAND, R. C., AND V. CHAMBERLAIN. 1987. Internal waves of the second vertical mode in a stratified lake. Limnol. Oceanogr. **32:** 29–42.

Received: 5 November 1999
Accepted: 17 April 2000
Amended: 19 June 2000